UNIVERSITY OF CALIFORNIA,
IRVINE

Time-Resolved Measurement of Vibrational Coherences in the Single Molecule Limit

THESIS

submitted in partial satisfaction of the requirements
for the degree of

MASTERS OF SCIENCE

in Chemistry

by

Steven Yampolsky

Dissertation Committee:
Professor V. A. Apkarian, Chair
Professor Eric O. Potma
Professor Craig Murray

2014

DEDICATION

With ideas it is like with dizzy heights you climb: At first they cause you discomfort and you are anxious to get down, distrustful of your own powers; but soon the remoteness of the turmoil of life and the inspiring influence of the altitude calm your blood; your step gets firm and sure and you begin to look - for dizzier heights.

-Nikola Tesla

To my parents, who provided for me all I needed to let my imagination and curiosity run wild.

TABLE OF CONTENTS

LIST OF FIGURES

ACKNOWLEDGMENTS

I would like to thank my advisor, Professor Ara Apkarian, for his continued guidance and unyielding patience. Thank you for taking a chance on someone who "liked to play with lasers" yet knew not a single thing about them a priori. I would also like to acknowledge these people for their collaboration in not only work, but in life as well;

- Kevin Crampton
- Hayk Zadoyan
- Dr. Patrick Z. El-Khoury
- Paulina Temple
- Mark Yampolsky
- Dr. Dmitry Fishman
- Amir Sadr
- Professor Eric Potma
- Dr. Desiré Whitmore
- Daniel Shemtob
- Alan Kante
- Dr. Eero Hulkko
- Dr. Wytze van der Veer
- Jeremy Garrett
- Dr. Michael Karavitis
- Peter Preston
- Ash Shamsian
- Professor Vladimir Mandelshtam
- Professor Sergey Nizkorodov
- Drs. Alex, Michael and Mrs. Ira Ushinsky,
- The Moroz family
- The Zubatov family

ABSTRACT OF THE THESIS

Time-Resolved Measurement of Vibrational Coherences in the Single Molecule Limit

By

Steven Yampolsky

Masters of Science in Chemistry

University of California, Irvine, 2014

Professor V. A. Apkarian, Chair

Time-resolved, surface-enhanced, coherent anti-Stokes Raman spectroscopy (tr-SECARS) is ideally suited for preparing and interrogating vibrational coherences on single molecules. We have succeeded in the first demonstration of this concept through measurements carried out on molecules attached to gold nanosphere pairs which act as plasmonic nano-dumbell antennae. The tr-SECARS traces provide unique signatures of coherent evolution in discrete ensembles. The signals are characterized by phase and amplitude noise, which can be cast in terms of amplitude probability distribution functions (PDF), which allow rigorous distinction between single, few, and many molecule coherences. We give a brief background on tr-CARS, the experimental system for carrying out tr-SECARS and the analysis of the results in terms of PDFs. The analysis makes it clear that we have, for the first time, observed the coherent vibrational motion of a single molecule.

Chapter 1

Introduction

Time-resolved coherent anti-Stokes Raman scattering (tr-CARS) is a powerful tool in the arsenal of nonlinear optical spectroscopy techniques used for preparing and later interrogating vibrational dynamics on the ground electronic state of a molecule.[1, 2] tr-CARS measurements are well documented for ensembles of molecules.[3–5] In the ensemble measurement, the observed signal strength is proportional to the number of irradiated molecules but is limited in information by the ensemble coherence time.[6] A measurement on a single molecule is not limited by this loss of coherent information, known as pure dephasing. This raises fundamental questions regarding the fate of the induced coherence. The coupling of the incident optical fields and resolution of the feeble single molecule response can be enhanced by the use of a plasmonic antennae.[7, 8] Plasmonic antennae in the form of two gold nanospheres in close proximity, are used to efficiently deliver optical fields to a molecule located at the junction between the spheres. The incident electric fields are delivered to the molecule through the excitation of the surface plasmons on the gold nano spheres. Radiative emission from the single molecule is enhanced for more efficient collection. The first part of the introduction will illuminate the information content in the tr-CARS signal and how to extract pertinent parameters therein. Secondly, the finer details of plasmonic enhancement

will be discussed. Upon a greater understanding of the experiment and its challenges the results will be described and analyzed, and later put into perspective for its place in the quantum world and the possible applications in, but not limited to quantum logic.

1.1 tr-CARS Observables

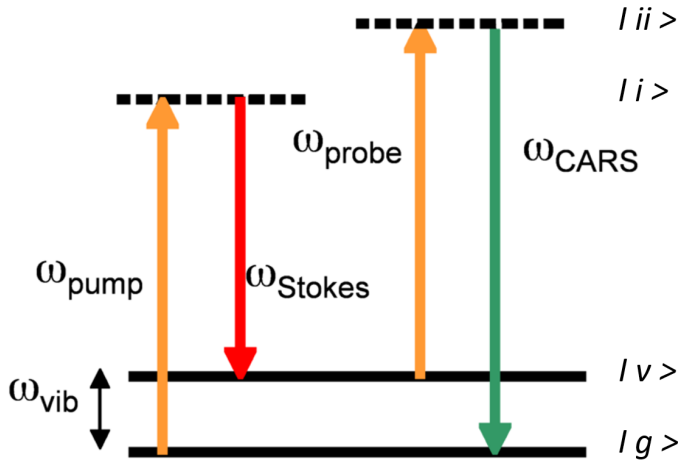

Figure 1.1: Jablonski representation of tr-CARS. The pump beam ω_p promotes electrons from the ground state $|g\rangle$ to an imaginary excited state $|i\rangle$, the Stokes beam ω_S then stimulates the electrons to vibrational eigenstates $|v\rangle = \omega_P - \omega_S$ where after Δt of evolution, the electrons are excited to another imaginary state $|ii\rangle$ (referred to in text by $|i'\rangle$) by the probe pulse ω_{pr}. From the final state $|ii\rangle$ the electrons spontaneously relax to $|g\rangle$ accompanied by the emission of an anti-Stokes photon $\omega_{AS} = \omega_p - \omega_S + \omega_{pr}$

Time-resolved coherent anti-Stokes Raman scattering(tr-CARS)[9] is illustrated in Jablonski representation in Figure 1.1. The preparation consists of action by a pump (ω_p) and a Stokes (ω_S) pulse, at time $t = \tau$ described classically;

$$E_p(t,\tau) = E_{0,p} e^{-(\frac{t-\tau}{\sqrt{2}\Delta t})^2} e^{-i\omega_p t} \tag{1.1}$$

with the Stokes pulse;

$$E_s^*(t,\tau) = E_{0,s} e^{-(\frac{t-\tau}{\sqrt{2}\Delta t})^2} e^{i\omega_s t} \tag{1.2}$$

where E_0 describes the amplitude of the field, ω, the carrier frequency (such that $\omega_p > \omega_s$), τ, the time at which the pulse acts, and Δt the variance of the pulse envelope, where the FWHM of the pulse is $2\sqrt{2\ln 2}\Delta t$, assuming a Gaussian envelope. A graph of a pulse in time, including its real, imaginary and envelope components is shown in Figure 1.2. The

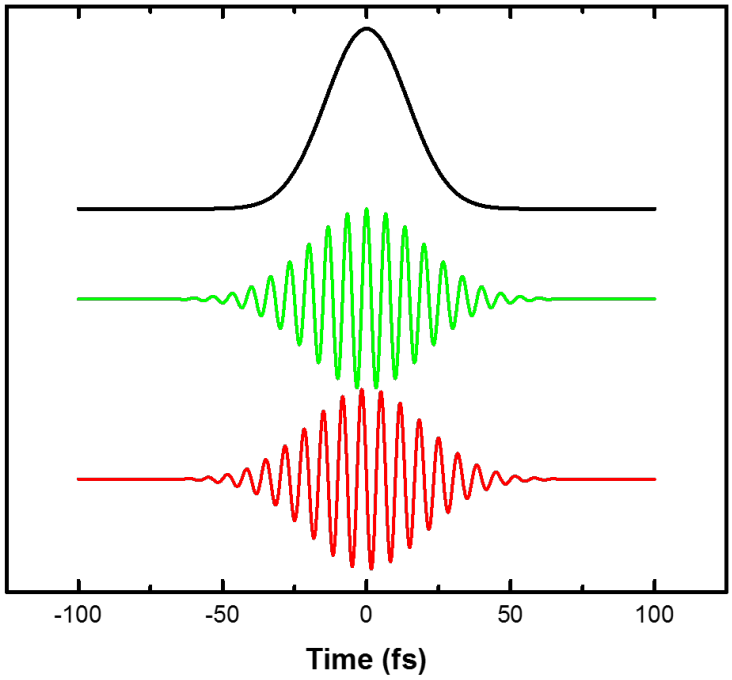

Figure 1.2: A Gaussian pulse with $\omega = 374$ THz (800 nm) and $\Delta t = 20$ fs with the imaginary (red), real (green), and intensity (black) components offset vertically

higher energy pump pulse promotes the ground state, $|\psi^{(0)}(x,0)\rangle$ of the system to an excited

$|\psi^{(1)}(x,t')\rangle$ [10], where;

$$|\psi^{(1)}(x,t')\rangle = -i\int_{-\infty}^{\tau_1} e^{-iH_{mol}(t)}\mu_{gi}(x)E_p(t,\tau_1)|\psi^{(0)}(x,0)\rangle dt \tag{1.3}$$

where H_{mol} is the Hamiltonian of the system and μ_{jk} is the transition dipole moment between j and k states. The longer wavelength Stokes pulse stimulates the amplitude down to create a vibrational superposition $|\psi^{(2)}(x,t)\rangle$ in the ground electronic state;

$$|\psi^{(2)}(x,t'')\rangle = -i\int_{-\infty}^{\tau_2} e^{-iH_{mol}(t')}\mu_{iv}(x)E_S^*(t',\tau_2)|\psi^{(1)}(x,t')\rangle dt' \tag{1.4}$$

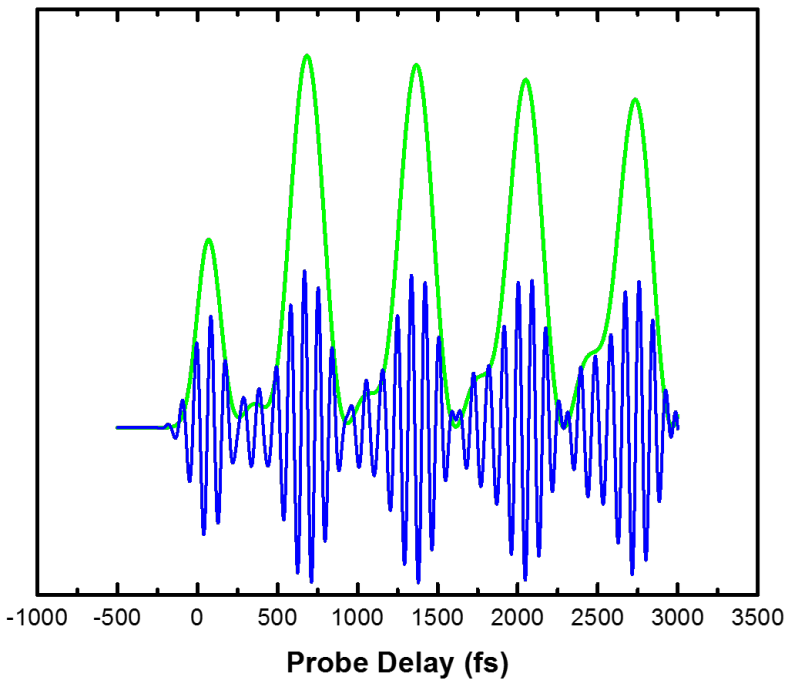

Figure 1.3: A vibrational wavepacket ψ consisting of four eigenstates prepared at $t = 0$ fs (blue) along with the density $|\psi^*\psi|$ of the wavepacket (green), where the oscillations, in green, are comprised of difference frequencies between the prepared vibrational eigenstates

A vibrational coherence $|\psi^2(x,t)\rangle\langle\psi^0(x,t)|$ is created. The evolution of $|\psi^{(2)}(x,t'')\rangle$ is de-

picted at early time in Figure 1.3. After some time-delay τ the vibrational coherence is interrogated by the action of a third probe (pr) pulse;

$$E_{pr}(t,\tau) = E_{0,pr}e^{-(\frac{t-\tau}{\sqrt{2}\Delta t})^2}e^{-i\omega_{pr}t} \tag{1.5}$$

which excites the vibrational wavepacket to another non-resonant or resonant excited state $|\psi^{(3)}(x,t)\rangle$;

$$|\psi^{(3)}(x,t''')\rangle = -i\int_{-\infty}^{\tau_3} e^{-iH_{mol}(t'')}\mu_{vi'}(x)E_{pr}(t'',\tau_3)|\psi^{(2)}(t'')\rangle dt'' \tag{1.6}$$

creating the tr-CARS polarization.[11] Integrating over the square of the polarization results in the measured signal;

$$S_{CARS}(t) = \int_{-\infty}^{\infty} dt|P^{(3)}(\tau)|^2 = \int_{-\infty}^{\infty} dt|\left\langle \psi^{(0)}(t)\,|\mu|\,\psi^{(3)}_{\mathbf{E}_p-\mathbf{E}_s+\mathbf{E}_{pr}}(t)\right\rangle + C.C.|^2 \tag{1.7}$$

from which the wavepacket can spontaneously relax to the ground state accompanied by the emission of an anti-Stokes(AS) photon. If the spontaneous emission is from a real state, a subsequent re-emission can occur shortly thereafter. The anti-Stokes photon contains information about the relative phase of the vibrational coherence for each time delay τ_3. The AS photon satisfies the energy conservation condition;

$$\omega_{anti-Stokes} = \omega_{pump} - \omega_{Stokes} + \omega_{probe} \tag{1.8}$$

In an ensemble, or a bulk medium, which contains a thick sample of polarizable material, the third order polarization will also have an associated momentum vector, which is also conserved;

$$k_{anti-Stokes} = k_{pump} - k_{Stokes} + k_{probe} \tag{1.9}$$

In a collinear mixing case, collection of the AS photon is background free when using three different color pulses or when the three pulses do not overlap in time. Spatial filtering is also possible when the wave vector momentum conservation is revisited in the BOXCAR geometry, where the three pulses are mixed non-collinearly.[3] To derive the time dependent signal the third order polarization for the CARS pathway is considered. [12] Note, this approach neglects certain contributions that may arise from pre-populated vibrational states, i.e. $\hbar\omega_p - \hbar\omega_S >> kT$. The measured third order polarization arises from the time ordered interaction of the three pulses;

$$\begin{aligned} P^{(3)}(x,t) &= \frac{-i}{\hbar^3}\sum_{givi'} p_g \mu_{i'g}(x) \int_{-\infty}^{t}\int_{-\infty}^{\tau_3}\int_{-\infty}^{\tau_2} (e^{-iE_{i'g}(t-\tau_3)}\mu_{i'v}(x)E_{pr}(\tau_3)e^{-iE_{vg}(\tau_3-\tau_2)} \\ &\qquad \mu_{vi}(x)E_s^*(\tau_2)e^{-iE_{ig}(\tau_2-\tau_1)}\mu_{ig}(x)E_p(\tau_1) + c.c.)d\tau_3 d\tau_2 d\tau_1 \end{aligned} \tag{1.10}$$

This expression integrates over the action of each time-ordered pulse and the subsequent evolution on the respective excited state. In the case of resonant CARS, the states denoted by i and i' (or ii) are real electronic eigenstates of the system where wavepacket evolution may occur and spontaneously emit in absence of a stimulating electric field.

The above description takes into account the possibility of evolving on all states. In non-resonant tr-CARS where states i and i' are imaginary states, no evolution can occur, hence further simplifications can be made. The action of the pump pulse at τ_1 occurs at $t = 0$, Due to the fact that state i is a virtual state, τ_2 must also be set to $t = 0$. The lack of resonance dictates that the optimum transition conditions are achieved when the pump and Stokes pulse overlap in time. The action of the probe pulse, in the non-resonant case, will only spectrally shift the relative phase of the evolving vibrations and give rise to the AS photon. By energy conservation the spectral distribution of $|\psi^{(2)}(x,t)\rangle$ is described by the

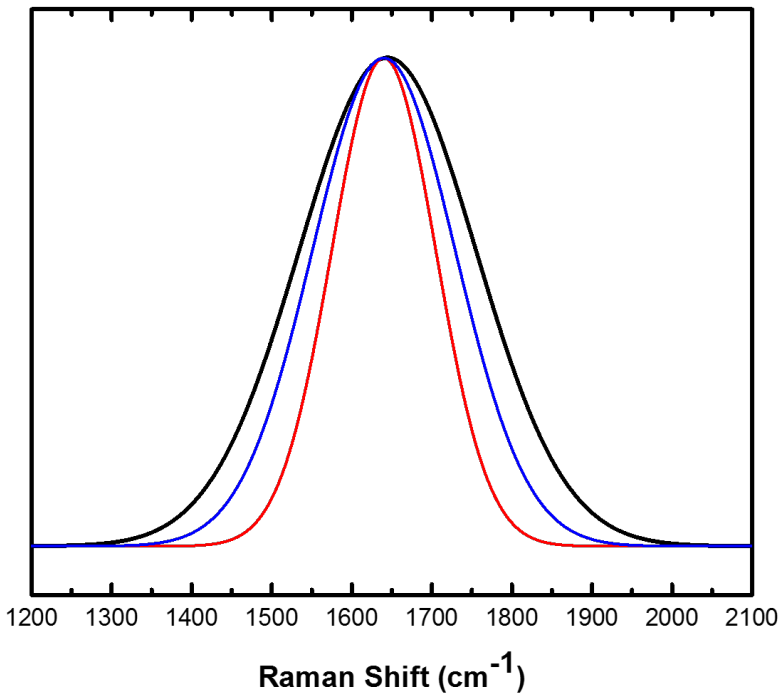

Figure 1.4: The pulses(pump in red and Stokes in blue), convolved in the spectral domain. Tuned by the difference between the pump and Stokes pulses, the convolution selectively excites vibrational eigenstates $E_v = \omega_p - \omega_S$ that fall within its spectral domain

spectral convolution of the E_{pu} and E_{Stokes} pulses depicted in Figure 1.4;

$$E(\omega) = \int_{-\infty}^{\infty} E_p(\omega') E_s^*(\omega - \omega') d\omega' \tag{1.11}$$

The vibrational wavepacket, prepared at $t = 0$ is the superposition;

$$\psi^{(2)}(x,t) = \sum_{i=1} \psi_v(x) a_i e^{-\imath E_i t} \tag{1.12}$$

where $\psi(x)$ is the spatial wavefunction with amplitude $a_i = E(\omega)\delta[\omega - E_i/\hbar]$ dictated by the two pulse convolution described in Eq. (1.11), E_i is the energy of the vibrational eigenstate

i. The evolving vibrational coherence $|\psi^{(2)}\rangle\langle\psi^{(0)}|$ is then interrogated by the time-delayed probe pulse. The time integration, Eq. (1.9), by a photodetector washes out the carrier frequency, and the signal is reduced to the sum of relative phases between the prepared vibrational eigenstates. For a two eigenstate superposition;

$$|\psi^{(2)}(t)|^2 = |\sum_{i=1}^{2} a_i e^{-i\frac{E_i}{\hbar}t}|^2 = (a_1 e^{i\frac{E_1}{\hbar}t} + a_2 e^{i\frac{E_2}{\hbar}t})(a_1 e^{-i\frac{E_1}{\hbar}t} + a_2 e^{-i\frac{E_2}{\hbar}t}) \tag{1.13}$$

Using $E = \hbar\omega$, the measured signal is reduced to;

$$\begin{aligned}
&a_1^2 e^{-i(\omega_1-\omega_1)t} + a_1 a_2 e^{-i(\omega_1-\omega_2)t} + a_2 a_1 e^{-i(\omega_2-\omega_1)t} + a_2^2 e^{-i(\omega_2-\omega_2)t} = \\
&= a_1^2 + a_2^2 + a_1 a_2 e^{-i(\omega_1-\omega_2)t} + a_2 a_1 e^{i(\omega_1-\omega_2)t} = \\
&= a_1^2 + a_2^2 + a_1 a_2 (cos[(\omega_1-\omega_2)t] - isin[(\omega_1-\omega_2)t]) \\
&+ a_2 a_1 (cos[(\omega_2-\omega_1)t] + isin[(\omega_2-\omega_1)t]) = \\
&= a_1^2 + a_2^2 + 2(a_1 a_2) cos[(\omega_1-\omega_2)t]
\end{aligned}$$

The signal is the beat frequency between the two vibrational bands above a constant background. In general, the coherence measurement, which probes the off-diagonal density matrix elements, describes the difference frequency between all excited vibrational bands. The measured quantity at any time delay is the sum over all transition frequencies squared. The finite linewidth of transitions implies a phase distribution in the evolving coherence. At early delay times, the phases can be described by a normal distribution function with a variance that is proportional to the delay time of the probe. At sufficiently large delay times the phase distribution becomes uniform and the expectation value of the phases goes to zero. This behavior is an inherent property of the ensemble known as pure dephasing, denoted by T_2^* [12]. The ensemble eigenstate bands are described by a homogeneous distribution, the

inverse width of which is the lifetime of the eigenstate T_1. In the above example, the eigenstates are spectral delta-functions, subject to no decay $T_1 \to \infty$. Typically, in a tr-CARS measurement on an ensemble, pure dephasing will scramble the measured phase long before the vibrational vibrational eigenstates decay. The overall decoherence time of the signal, T_2, is a combination of these two factors;

$$\frac{1}{T_2} = \frac{1}{2T_1} + \frac{1}{T_2^*} \tag{1.14}$$

1.2 tr-SECARS

The tr-CARS signal is proportional to n^2, where n is the number of molecules in the excitation volume. [13] To execute a tr-CARS measurement on a single molecule, the one photon response must be enhanced. Surface enhanced Raman scattering (SERS) has enabled detection of trace quantities of molecules that are highly diluted in their local environments. [14–17] SERS has been extended and studied in various configurations: thin films [18, 19], colloidal particles [20, 21], and nanowires [22]. The enhancement of the detected vibrational fingerprint is made possible by simultaneously excited plasmon modes of a nearby metallic structure. In the presence of an electric field, a metal nanosphere's surface electron density will oscillate at the frequency of the incident electric field [23, 24]. However, when there are two spheres in very close proximity, given the optimum incident field polarization, a dipole is created at the nanometer junction of the two spheres that is much greater in amplitude and oscillates with the incident electric field. The focused excitation junction is roughly a few molecules in size, allowing for a greater probability of catching a single molecule in action. [25, 26] In addition to the concentrated excitation, the emitted anti-Stokes photon from the molecule located in the junction, drives the collective electrons of the spheres. The anti-Stokes radiation is thus amplified proportional to the oscillator strength of the plasmon.

If the incident electric field satisfies the surface plasmon resonance condition of a particular material and structure(in this case, a pair of spheres), then the amplitude of the field is also significantly increased at the junction(between the spheres).[27, 28] Raman intensity scales as $|E_0|^2$, in SERS, this relationship is $|E_0|^4|$ as both the driving field, and the molecular response is enhanced. Following the enhancement of two fields in SERS, we expect the CARS photon, a phenomenon involving four fields, to have $|E_0|^8$ enhancement.[29] Surface enhanced coherent anti-Stokes Raman scattering was first measured on a plane metal silver surface by Shen *et al* in 1984.[30] Upon examining a plane silver surface with the CARS method, a 992 cm^{-1} vibration was observed from a benzene molecule. Shortly thereafter Chew and coworkers [31] predicted an enhancement factor of SECARS of 10^{12} when the pump and stokes beams were both perpendicularly oriented to the metal plane, but a 10^{21} enhancement factor when the fields were cross polarized. This magnitude of enhancement factors have not yet been realized experimentally. Very recently, an experimental SECARS enhancement factor of $3.6x10^7$ has been observed from a self-assembled monolayer of benzenethiol on a silver coated substrate.[32] Voronine *et al* used a colloidal solution of gold nanoparticles to obtain the tr-SECARS signal of a low concentration pyridine solution.[33] Naturally, after successful execution of a tr-SECARS measurement on a dilute molecule, the stage is set for such a measurement to be executed in the single molecule limit.

Chapter 2

tr-SECARS Experiment

2.1 Experimental Setup

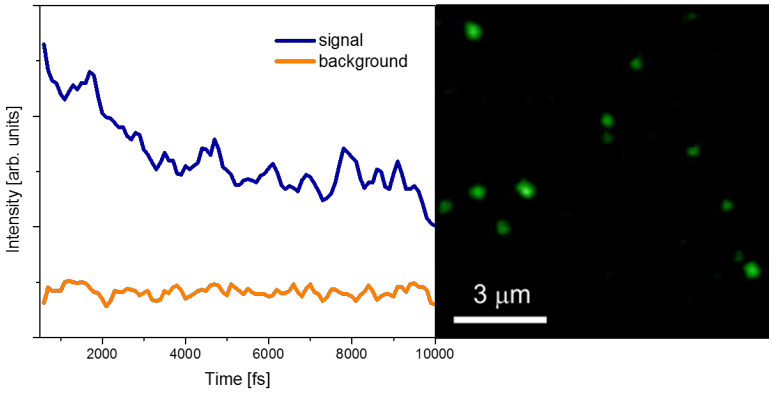

Figure 2.1: Time trajectories are taken from structures confirmed by SEM and Raman to be SERS-active dumbbell structures (green dots in CARS imaging data on the right) show time dependent oscillations, whereas the dark region (silicon nitride membrane), shows no modulation as a function of time.

The single molecule samples are purchased from Cabot Security Materials. The structure consists of two gold spheres, roughly 90-100 nm in diameter, immersed in trans-bipyridyl

ethylene. The entire system is enclosed in a 70-80 nm thick Silicon oxide shell. The shell is used to better ensure structural integrity of the system, and as a heatsink into which peak power excitation can dissipate. The sample is diluted to the desired concentration, and then spin coated or drop cast onto a silicon nitride TEM grid (Ted Pella). The silicon nitride is roughly 20 nm thick to ensure minimum scattering background. The spin coated sample is then taken to the SEM for coarse characterization of the available candidate structures for the experiment. Though SEM only offers a rough picture, ideal dumbbell structures can be identified and later probed. The selected candidates are then taken to a high numerical aperture Raman microscope to be characterized for Raman activity of the trans-bipyridyl ethylene. A few molecules with significantly apparent Raman spectra per grid are then tagged and taken to the time resolved system. The time resolved system is pumped by a commercial femtosecond titanium sapphire laser (Spectra Physics Mai Tai). The output is frequency doubled to pump a tunable optical parametric oscillator (Radiantis Inspire OPO) tuned to be offset from the fundamental frequency by $1627 cm^{-1}$. The OPO output (714 nm) along with the residual fundamental are compressed in time with a double pass prism compressor to achieve transform limited pulses. The OPO output split into two arms, one to be incident in time with the residual 809 nm and create the vibrational superposition, and another on a digitally controlled delay to probe the vibrational coherence created by earlier pulses. The three arms are overlapped collinearly and directed to a commercial microscope (Olympus IX-73) equipped with a Fluoview (FV1000) imaging system. The beams are focused into the sample by a 60x oil immersion objective with a numerical aperture of 1.42. The spot size of the beam is diffraction limited to 400 nm at the focus. The back scattered anti-Stokes photons are filtered out of the path by a dichroic mirror and collected with a monochromator CCD or photomultiplier tube (PMT). The forward scattered signal is also filtered and collected by a PMT. The Fluoview system can raster the beam to create an image of the sample in typically a 125 μm by 125 μm image with variable resolution and integration time per pixel. The luxury of having mirrors capable of rastering in the X and Y plane of the sample allow

us to image an entire 100 μm x 100 μm grid, while the photomultiplier tubes record an intensity to each corresponding X and Y value. The gold nanoparticles are imaged using electronic CARS response of the surface plasmon modes[34, 35] shown in Figure 2.1 on the right. The time trace corresponding a gold nanosphere (dimer) structure show oscillations, while the dark regions of the image, consisting of the 20 nm silicon nitride membrane, shows a constant level throughout all the time traces, with a small amplitude noise arising from the PMT pulse height distribution. Samples are either zoomed into and collected rastered over quickly with the signal detected by monochromator/CCD, or alternatively, the whole 100x100 micron grid can be imaged using the PMTs. Measurements are made at iterated time delays of the probe pulse and displayed in the following section.

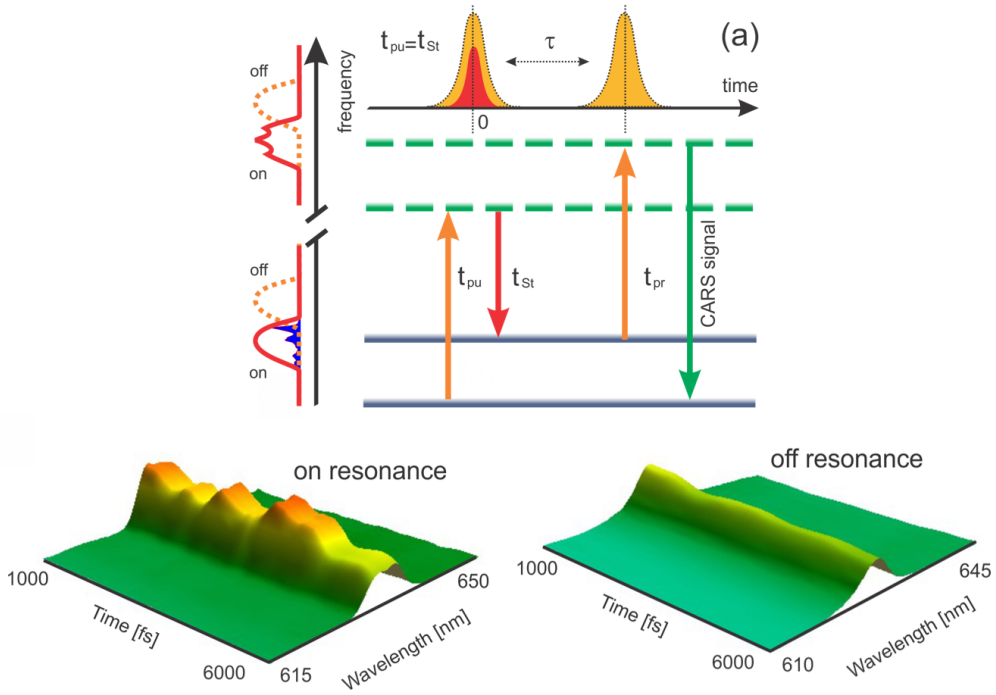

Figure 2.2: When the pump and Stokes pulse spectral convolution is tuned to overlap with the vibrational eigenstates (on resonance) modulations proportional to the difference frequencies of vibrational eigenstates are observed, whereas if the convolution does not overlap with the eigenstates (off resonance) no modulation activity is observed

Three measures were taken to ensure that the signal we collect is in fact tr-CARS. Firstly, the preparatory bandwidth was tuned to a region with no peaks in the Raman spectrum. Assuming the signal is CARS, if the bandwidth overlaps with vibrational bands, the time resolved measurement yields the difference frequency of all prepared bands oscillating in time. So if no bands are prepared within the convolution, no oscillations should be seen in the time delay. Such is the case in Figure 2.2. Here we see oscillations resembling 1 ps periods, analogous to the separation between the mean vibrational frequency in the Raman spectrum of the dimer. In the non-resonant case, a flat background is seen at all delays. The constant background arises from the time zero response of the gold nanoparticles. The level is constant across all delays because while the response of the gold is not long lived, due to the degenerate spectrum of the pump and probe beams, the pump beam may act twice at time zero and generate an anti-Stokes photon before the system even evolves. Future experiments will include three independent colors so as to avoid the problem of signal contamination making the measurement truly background free.

Another test used to determine the validity of the CARS experiment is comparison of the negative versus positive time traces. Measurements at negative time probe the coherence before the coherence is prepared.[36] Given that there is no coherence to interrogate, there should be no oscillations or amplitude related to the vibrations evolving in time. In Figure 2.3 low noise modulations are shown before time zero, with high amplitude oscillations resembling a 1 ps period, establishing that the prepared vibrational coherence is indeed being probed, atop a constant gold time zero response.

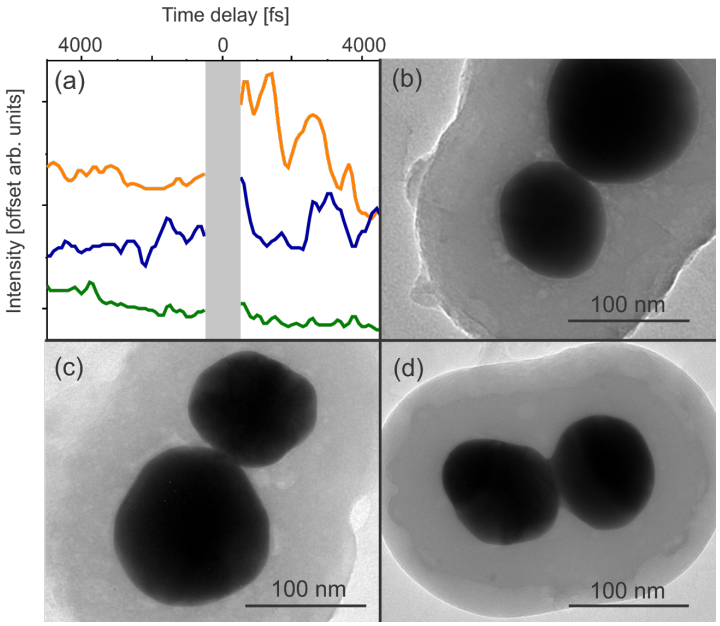

Figure 2.3: Time traces of individual dumbbell structures that are SERS active (TEM images and after irradiation in (b),(c),(d)) show little to no modulation at negative time (before superposition is prepared), and exhibit modulation activity with a period of 1 ps after the superposition is prepared (orange and blue trace). SERS inactive structures show no modulation activity at negative and positive time (green trace)

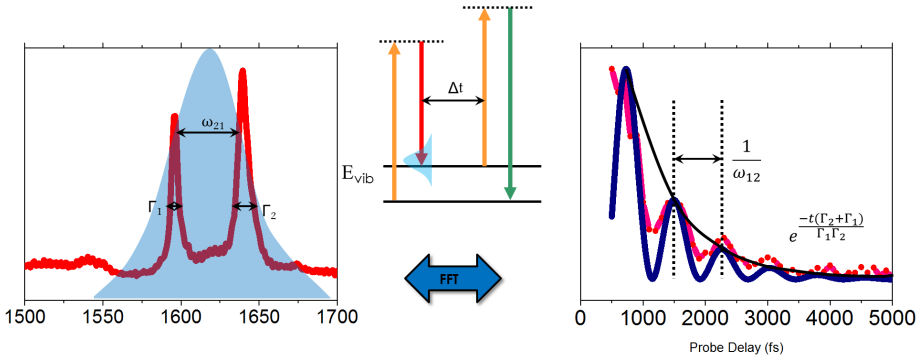

Figure 2.4: (Left) an ensemble Raman spectrum (red) of trans-bipyridyl ethylene with a two pulse(Pump+Stokes beams) spectral convolution (blue). (middle) Jablonski representation of tr-CARS, (right) a tr-CARS trajectory of bulk trans-bipyridyl ethylene (red) with an FFT of the bulk Raman spectrum (blue) shown on the left.

2.2 tr-CARS in the Single Molecule Limit

For the case of an ensemble, by extracting a vibration's central frequency and homogeneous linewidth, as well as the difference in vibrational frequencies prepared under a two-pulse convolution, the tr-CARS trace can be reconstructed via a Fourier transform. The time trace consists of oscillations, with frequencies equal to the difference frequencies of the states prepared. The signal will contain beats with a modulation depth determined by the amplitudes a_i (see Eq. (1.12)). of the vibrations from the Raman spectrum. The oscillations will decay as a function of the inverse linewidth of the vibrational bands. In addition to the dissipation of the hot vibrational state, the decay of the oscillation depth will be accelerated by pure dephasing, or the impact of collective oscillations of many molecules simultaneously, each with its own relative phase. Two C=C stretching modes belonging to the pyridine ring breathing mode and the ethylinic stretch of BPE [37] centered at $1600\ cm^{-1}$ are the focus of the tr-SECARS measurement. The ensemble trans-bipyridyl ethylene Raman spectrum shows 2 homogeneous vibrations within the two pulse convolution window with a separation of $33\ cm^{-1}$ and a width of $5\ cm^{-1}$. A Fourier transform of the ensemble Raman spectrum agrees perfectly with the experimental trace, which decays over the course of a few ps (Figure 2.4). Thus all the information contained in the tr-CARS measurement of an ensemble can be obtained by performing a more trivial Raman measurement.[38] However, the reasoning above cannot explain the tr-CARS trace in the case of a single molecule.

The SERS spectrum in Figure 2.5 of the single nanoparticle shows vibrational bands approximately at the same frequencies as the ensemble trans-bipyridyl ethylene spectrum. The gold nanoballs that encase a molecule (or a few) in their junction contain peaks with a Gaussian lineshape three times larger in width than the ensemble Raman peaks.[39] The inhomogeneous lineshape is indicative of spectral diffusion that is too fast to be observed in the time frame necessary to obtain significant signal to noise in the spectrum. When the spectra are

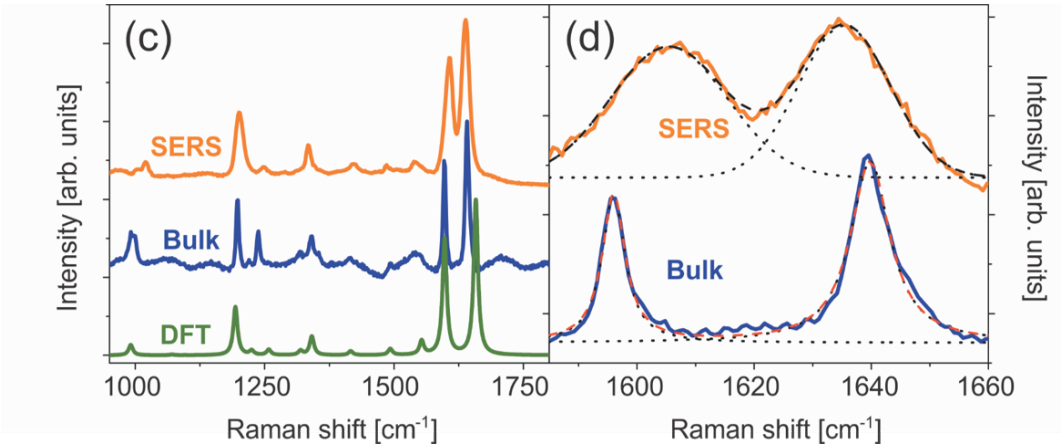

Figure 2.5: BPE in a SERS active dumbbell(orange), in bulk (blue) and calculated (green). (right) Close up of the vibrations(orange from SERS active structure, blue from Bulk BPE) that were subsequently probed with tr-CARS

collected sequentially with a lower integration time, benign traces of the spectral diffusion and amplitude modulation can be observed in Figure 2.6.

This behavior is the hallmark of a few, or possibly a single molecule. As a consequence, when performing a tr-CARS measurement, the vibrations prepared and subsequently probed during one pulse, may diffuse slightly in the preparation and probing of the next pulse. If the single molecule time trajectory could be extracted from the Raman spectrum, it would dictate that the single molecule time trace would decay much faster than the ensemble due to the 15 cm^{-1} linewidth of the vibrations, making the tr-CARS method redundant. Furthermore, distinguishing a single molecule from a few molecules in the frequency domain (Raman) is not trivial as both exhibit inhomogeneous vibrational bands with indiscernible characteristics. Only gold nanoballs that showed a Raman spectrum with features that resembled single or few molecule behavior were used in the tr-CARS measurements.

All tr-CARS measurements showed a signal that does not decay within the time prescribed by the width of the SERS-active gold nanoball structures. One particular trace is depicted in Figure 2.7 in green. The signal was fit (red trace) with four vibrational lines having a width

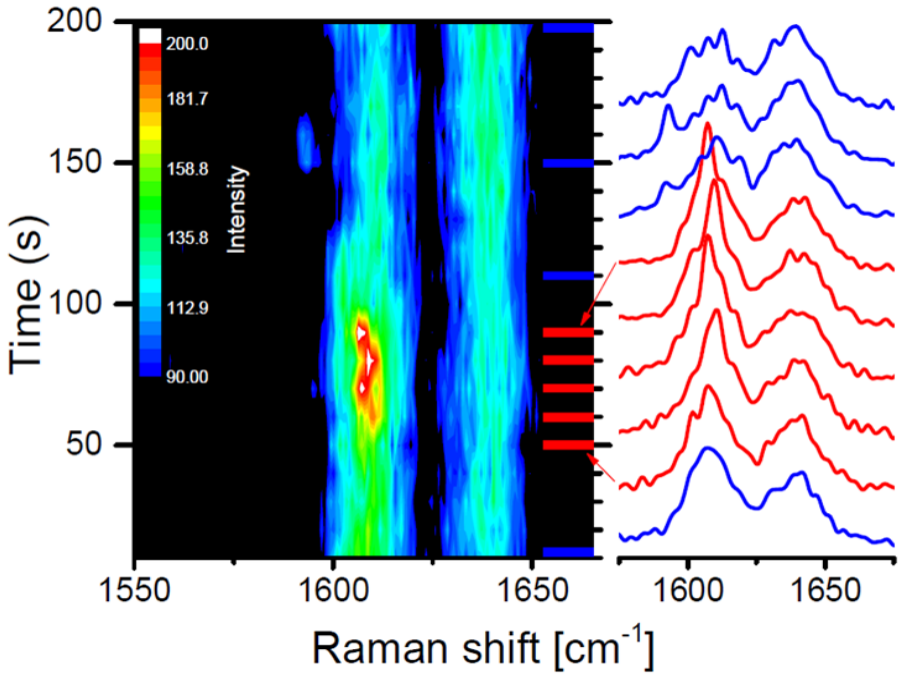

Figure 2.6: Raman spectra of a SERS-active dumbbell structure acquired sequentially in 10 s periods for 200s, with select spectra at various points in time (right). Modulations in peak width and intensity and mean frequency can be observed occurring on the acquisition time scale.

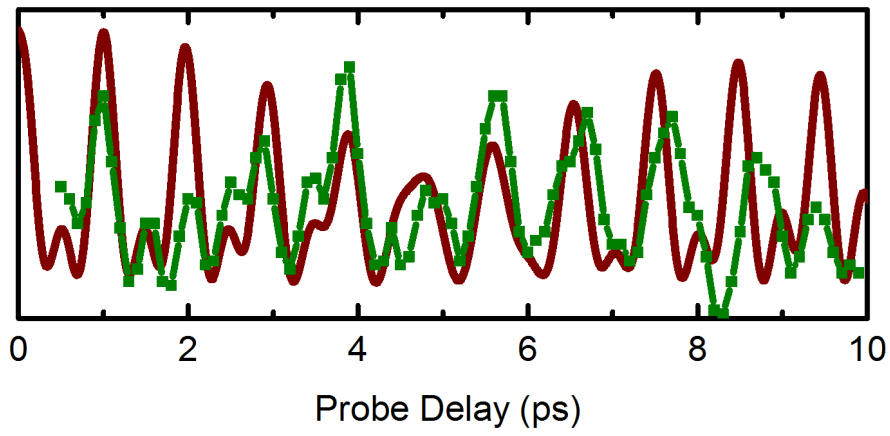

Figure 2.7: tr-CARS measurement on a SERS active dumbbell (green) shows distinct quantum beats, and can be simulated with good fidelity via FFT of four discretely defined vibrational eigenstates (red).

of 0.1 cm^{-1}. The slow beat was reproduced by having two vibrations, which appear briefly in the 1580 cm^{-1} region in the meandering Raman trajectory in Figure 2.6. The faster feature was produced by having one of these transient lines (from the meandering slide) beating against one of the main bands present in the ensemble and the dimer spectrum 1647 cm^{-1}. The 1 ps beat feature was reproduced by the two main vibrations 33 cm^{-1} apart. While the main features of the trace were reproduced, the SERS spectra show that in reality, the vibrations are much wider than the simulation prescribes.

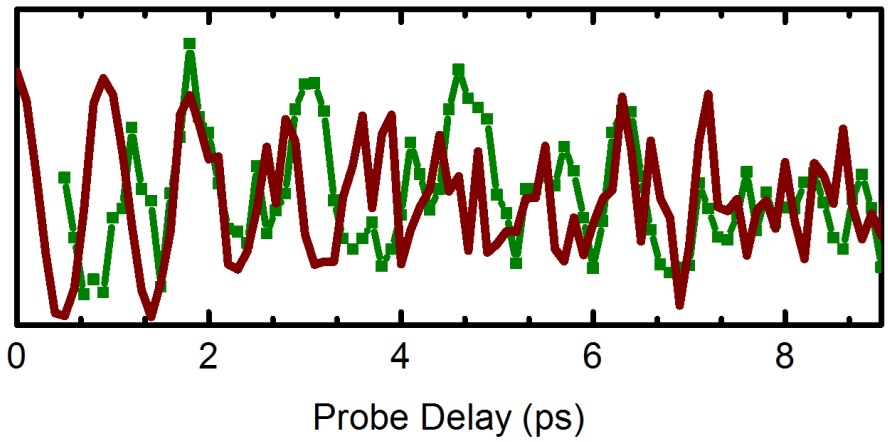

Figure 2.8: tr-CARS measurement on a SERS active structure (green) shows distinct quantum beats at early times, which recede into phase noise at later delay times. The fit (red), is one stochastic manifestation of phase noise that arises from a randomized shift δ from Eq. (2.2)

A more typical time trace is depicted in Figure 2.8 (green trace), where the 1 ps oscillation emerges at early delay times, with some noise, and eventually recedes to a smaller amplitude modulation around approximately $\frac{1}{2}$ the maximum amplitude at the time of preparation. This signal cannot be fit with the previous static narrow vibrational width model. However, if a small shift is added to the mean vibrational frequency to account for the spectral diffusion observed in the SERS Spectra, the noisy features, and the decay of the oscillation to noise can be reproduced. This shift from the mean vibrational frequency, is selected randomly upon

preparation, from within a normal distribution that matches the shape of the Gaussian lineshapes observed in the SERS spectra of gold nanoballs.

Here we depict the general model for the simulation used to replicate the experimental time traces;

$$S(t) \propto \frac{1}{M}\sum_{m=1}^{M}|\frac{1}{NV}\sum_{n=1}^{N}\sum_{v=1}^{V}a_{n,v}e^{-\imath\omega_{n,v}t}|^2 \tag{2.1}$$

where S is the signal over time which results from summing over N, the number of photons collected, M, the number of molecules, and V the vibrational eigenstates. For the time being, the number of photons collected is set to 1 for simplicity. In the case of one molecule and two vibrations, the above equation yields the trivial example depicted in the CARS theory section; a summation of a constant with a difference frequency oscillation. In order to simulate a time trajectory similar to the experimental traces, the spectral diffusion from the mean vibrational frequencies must be accounted for. A shift, $\delta_{n,v,m}$, of the bands is included, and can be random within a predefined normal distribution described earlier;

$$S(t) \propto \frac{1}{M}\sum_{m=1}^{M}|\frac{1}{NV}\sum_{n=1}^{N}\sum_{v=1}^{V}a_{v}e^{-\imath(\overline{\omega}_{v,n}+\delta_{m,v,n})t}|^2 \tag{2.2}$$

Upon further simplification;

$$
\begin{aligned}
S(t) \propto \quad & \frac{1}{N}\sum_{n=1}^{N}|\frac{1}{V}\sum_{v}^{V}a_i e^{-\imath(\omega_v+\delta_{v,n})t}|^2 \\
&= \frac{1}{4N}\sum_{n=1}^{N}|a_1|^2+|a_2|^2+2a_1a_2cos[(\omega_{21}+\delta_2-\delta_1)t] \\
&= \frac{1}{4N}\sum_{n=1}^{N}|a_1|^2+|a_2|^2+2a_1a_2cos[(\omega_{21}+\Delta)t]
\end{aligned}
$$

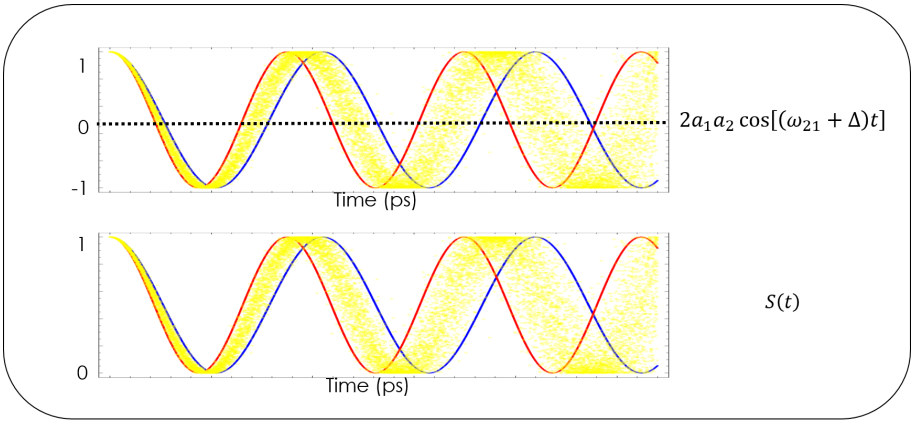

Figure 2.9: Simulation of the $2a_1a_2cos[(\omega_{21}+\Delta)t]$ (top) and the $S(t)$ (bottom) from Eq. (2.2) evolving in time. The red line represents the fastest beat frequency while the blue line represents the slowest. The yellow region in between indicates all possible values that can be measured in one stochastic trajectory.

Δ is introduced to highlight the covariance of the frequencies of the two states that are being measured.

To better illustrate the behavior of the covariance, an example with two excited vibrations is considered; a case with the smallest difference frequency and a case with the largest difference frequency within the normal distributions of the vibrational bands is illustrated in

Figure 2.9. The two cases provide an outline for all possible time traces that can be obtained when performing a tr-CARS measurement on this specific molecule. It is apparent that as the time between the preparation and probing increases, the possible intensities that can be obtained as a function of the "random" shifts of the vibrational frequencies increases. As the phase angle between the faster and slower oscillations reaches π all intensities in the oscillation depth are possible but occur within a normal distribution. Moreover, as the time is increased further, the phase angle will wrap 2π and the distribution, or the likeliness of measuring any phase becomes equal.

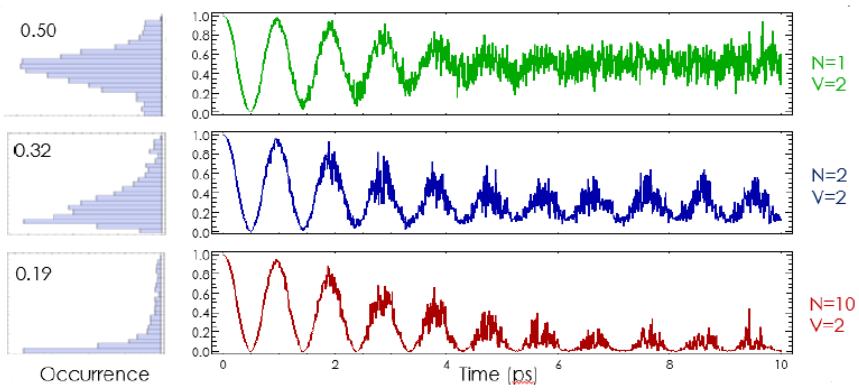

Figure 2.10: tr-CARS trajectories simulated for one (green), two (blue), and ten (red), molecule system(Eq. (2.2)), each prepared with one difference frequency and measured with 10 photons per delay. As the number of molecules prepared is increased, the onset of pure dephasing becomes more evident. On the left are probability distribution functions (PDF) for each time trace. The shape and the first two moments of these distributions is characteristic of the number of molecules prepared.

If a one molecule, two vibration system subject to phase shifts is prepared, and measured once only per delay (one photon gathered), the cosine term will yield the full range of -1 to 1 when $\tau >> 0$ and when incident on a photodetector (squared) will yield one value in the range of 0 to 1. The average of many measurements at later times where each measurement could be any random value from 0 to 1 will be 1/2. If two molecules with two vibrations are prepared, having the sum of two cosine terms squared will yield a value of 1/4 when

averaged over many measurements at large delay times. The one, two, and 10 molecule superposition is depicted in Figure 2.10. As the number of molecules prepared increases, so does the number of cosine terms in the molecular response function. The expectation value of many cosine terms with random phases is 0. Upon squaring the sum of many cosines the measured phase at later times is also expected to be 0. Thus, if many measurements are averaged, a mean value characteristic of the number of molecules and vibrations prepared can be obtained. The value is proportional to $\frac{1}{NV}$. For example, a single molecule, prepared with 2 vibrations, averaged over many measurements will converge to $\frac{1}{2}$ at a delay when the phase angle spans a uniform distribution. Note that the opposite case, where 1 vibration is prepared on two molecules is not possible, as the coherence of one vibration will not yield a time dependent oscillation. A single molecule tr-CARS trajectory does not decay by pure dephasing, but instead recedes into phase noise, which carries a characteristic mean.

The phase noise will manifest itself differently each time the simulation is computed or an experiment is performed. Therefore the fitting of the simulated phase noise to an experimental single molecule signal results in purely qualitative information. Amplitude histograms of the time traces can be made; and quantitative correlations extracted from the mean and variance of the histogram. These moments are characteristic to the number of photons collected, as well as the number of vibrational bands and the number of molecules prepared. If the number of photons collected from the system is large, then the variance of the histograms will be small. The mean can discern, most accurately between the single and many molecule case. The mean will approach 0 for the many molecule case, and converge to $\frac{1}{2}$ for the single molecule case(on a normalized scale of 0 to1). In general, for any number of N and V, the signal will converge to $\propto \frac{1}{NV}$. Coupled with a high number of collected photons, this relationship will be more precise. As V is increased, it becomes hard to discern the "many" molecule case from the "many" vibrational eigenstate case. As a result, the histogram analysis can accurately discern a single molecule signal for an ideal two vibrational eigenstates

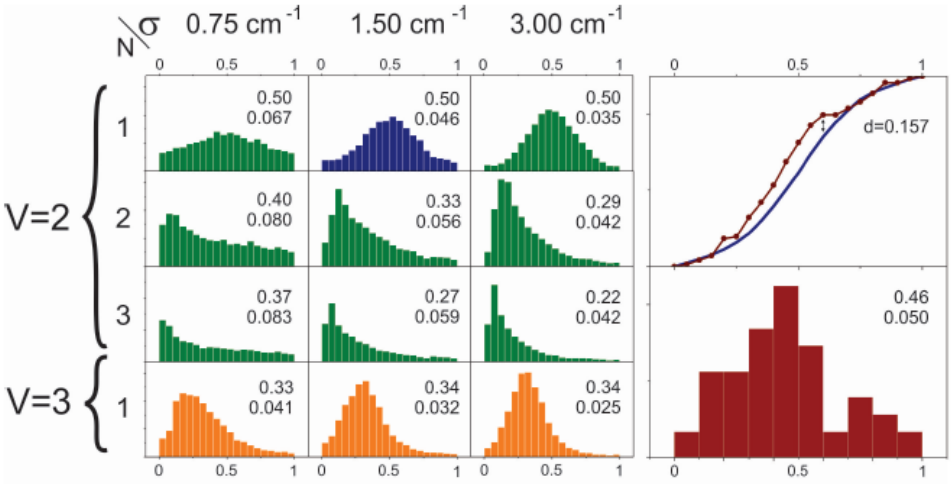

Figure 2.11: Probability distribution functions (PDF) generated using Eq. (2.2) for different numbers of molecules (N), vibrational eigenstates (V) and variance of spectral fluctuations (δ) On the right (red) is the PDF for the tr-CARS trace shown in Figure 2.8. The experimental PDF, along with mean and variance, uniquely match their simulated counterparts containing the parameters N=1, V=2, and $\delta = 1.50$ cm^{-1}. The experimental cumulative distribution function (CDF; red dots in the top right) and the theoretical CDF made from the PDF with blue bars are also indicated. The Kolmogorov-Smirnov(KS) test indicates a maximum distance of $d = 1.57$ between the theoretical and experimental CDFs. This d value translates into a 99% likelihood that the experimental data represents the evolution of a statistical two-state superposition on a single molecule.

contributing to the coherent phase correlation.

Simulation histograms for $V = 2, 3$ and $N = 1, 2, 3$ have been made in Figure 2.11, having covariance values of .75 cm^{-1}, 1.5 cm^{-1}, and 3 cm^{-1}, alongside histograms of experimental traces. The simulations from which the histograms have been generated, have been oversampled for a step size of 1 fs whereas the experimental traces were collected with 100 fs time steps. It is apparent that the experimental distribution matches closely to the histogram that was generated from one molecule with two vibrations and covariance of 1.50 cm^{-1}. Depicted in Figure 2.12 are two more time traces of the many that were collected. The first depicts

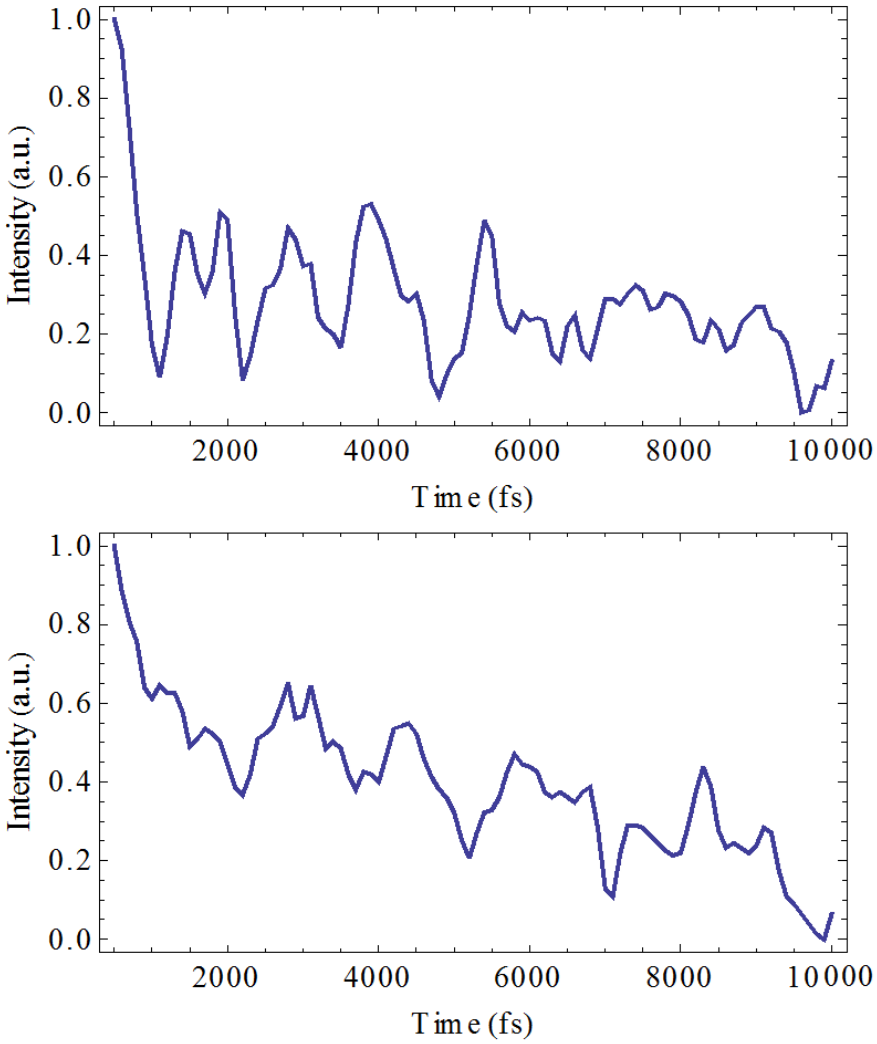

Figure 2.12: Two tr-CARS traces from other SERS active nanostructures. The top trace depicts distinct quantum beats at early times and recedes into phase noise albeit a small artifact at early time believed to be part of the three pulse correlation centered around $t = 0$ fs. The bottom trace shows signs of convergence to 0 as the probe delay is increased, indicating the preparation of more than one molecule.

a similar situation to the earlier experimental trace (Figure 2.8), albeit a small amplitude drop at early time. This feature could be an artifact of the interference between the pump and probe pulses around time zero. If those data points are omitted, the histogram also matches that of one molecule, two vibration model, with 1.5 cm^{-1} covariance. In the second case, there is an exponential decay and then the signal stays relatively flat, with ps features that appear to be the indication of two prepared vibrations 33 cm^{-1} apart. While the ex-

ponential decay is indicative of a large number of molecules within the interaction volume, the ensemble, as shown earlier, does not survive beyond a few picoseconds. Upon the loss of the ensemble coherence, the single molecule coherence persists.

The amplitude histograms can be made more accurate by averaging over a set of measurements on different dumbbells. We cannot add together the stochastic time trajectories, however, we can combine their histograms to improve statistical significance of the measurement set. Three trajectories were picked for each case of a single, few, and many (green, blue, and red PDFs in Figure 2.13). The sorting was done by the mean values of their respective PDFs. The PDFs corresponding to the green blue and red traces were combined to broaden the number of samples composing each respective summed PDF. The generated histograms can be transformed into cumulative distribution functions (CDF) for a more rigorous non-parametric analysis using the Kolmogorov-Smirnov(KS) test. This is done in order to compare the CDF of the simulation histograms to those that appear to be from single, few, and many molecules. The KS test uses a two sample comparison to provide correlation between two CDFs with the same number of elements using the distance between the two functions at any given element;

$$d = Max|F_i(x) - F_i'(x)| \tag{2.3}$$

where F_i and F_i' represent the experimental and simulated CDFs and i signifies the specific element in the CDFs. The KS test gives 99 % confidence probability if d does not exceed a critical value of 0.162 for a sample consisting of 100 elements. From a comparison of simulated vs experimental CDFs with their largest d shown in the respective comparison in the Figure 2.13. It can be seen that for the single, few, and many molecule case, the simulation and the experimental data exhibit statistical certainty with respect to their assignment.

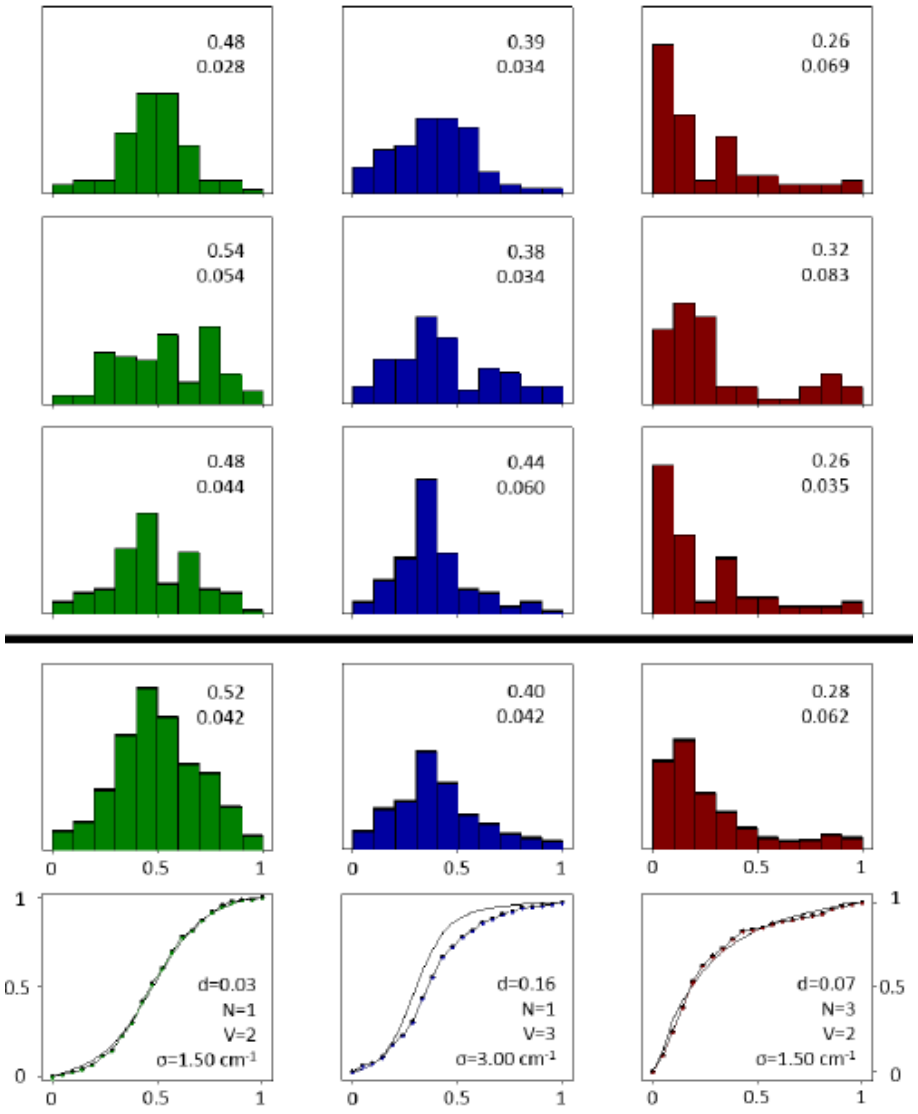

Figure 2.13: Probability distribution functions for tr-CARS traces obtained from nine different nanosphere structures. The mean and the variance of each distribution is also indicated. The PDFs are sorted by color based on their moments. The averaged PDFs appear in the fourth row, along with their CDFs in the fifth row. The CDFs are compared distribution functions generated from stochastic trajectories for the indicated number of molecules, vibrational eigenstates and their spectral covariance (N,V, and σ respectively). In all three cases, the measured distance d (Eq. (2.3)), is less than 0.162, indicating a 99% certainty of the assignments.

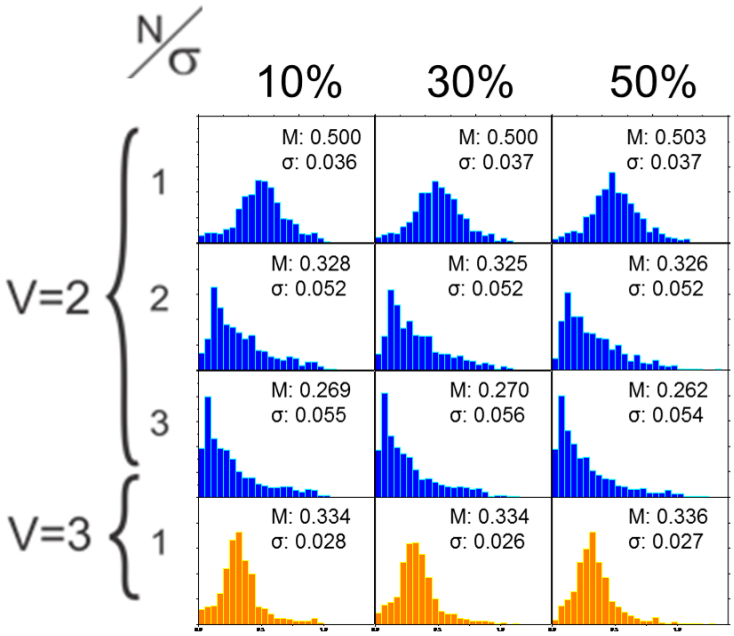

Figure 2.14: Amplitude noise (10, 30, and 50 % respectively) distributions generated for a various cases of molecules (N) and vibrations (V). With increasing amplitude noise, little to no change can be observed to the shape of the distribution, nor its first two moments as indicated in each row in the top right corner.

The histograms prove as an adequate characterization method for the phase noise on the vibrations prepared on a few molecules. Another source of noise that was not considered in the above analysis is amplitude noise. However, with the inclusion of amplitude noise from 10 % to the 50 % range. the shape of the distributions remains largely unchanged (see Figure 2.14). In the time trace picture, when measuring the difference frequency, the amplitude noise manifests itself at the peaks of the oscillations, thereby spreading the high intensity counts of the histograms to values above the normalized range. But the counts on the lower intensity remain unchanged.

When the tr-SECARS is combined with the histogram analysis, the difference between a single molecule and the many molecule case becomes trivial to discern quantitatively using the KS test, and traces of single molecule dynamics can be singled out and identified with

statistical certainty.

Chapter 3

Conclusions and Future Work

Here we present the first measurements that follow the evolution of a vibrational coherence on the ground state of a single molecule under ambient conditions. tr-SECARS was used to prepare a vibrational superposition of two vibrational bands, and a third pulse probed the phase correlation between the hot vibrational states as they evolved in time via a spectrally filtered, anti-Stokes photon. Plasmonic enhancement in the form of two gold nanospheres was employed to bring the single molecule response to a measurable level via use of amplification and subsequent broadcasting of the single molecule signal from the junction. The two nanospheres serve as a viable tool to interrogate single or few molecule entities and have been shown to endure the peak power of ultrafast pulses. Real time monitoring of vibrational evolution has been shown on the ground electronic state. Such a measurement can be extended to prepare and probe a coherence on multiple electronic states of a single molecule, with the possibility of complete quantum state reconstruction.[40, 41] Coherent manipulation of quantum bits has been demonstrated using a pair of phase-locked pulse pairs.[42, 43] Quantum bit manipulation is possible on the preparation, evolution, and interrogation steps of electronically resonant FWM. [44–46] However, this has yet to be demonstrated the single molecule limit. Proof of coherent evolution on a single molecule is a stepping stone to such

applications.

Bibliography

[1] Kiefer et. al. *J. Raman Spec.*, 32:771, 2001.

[2] W. Kiefer M Schmitt; G. Knopp, A. Materny. *Chem. Phys. Lett.*, 270:9, 1997.

[3] Karavitis et. al. *J. Chem. Phys.*, 114:4131, 2001.

[4] Segale et. al. *J. Chem. Phys.*, 135:024203, 2011.

[5] Senekerimyan et al. *J. Chem. Phys.*, 127:8, 2007.

[6] J. R. McDonald A. B. Harvey W. M. Tolles, J. W. Nibbler. *Appl. Spectrosc.*, 31:253, 1977.

[7] A. McQuillan M. Fleischman, P. Hendra. *Chem. Phys. Lett.*, 26:163, 1974.

[8] M. B. Rashke R. L. Olmon. *Nanotechnology*, 23:444001, 2012.

[9] Y. Silberderg N. Dudovich, D. Oron. *Nature*, 418:512, 2002.

[10] Prior et al. *J. Chem. Phys.*, 115:8440, 2001.

[11] Prior et al. *J. Chem. Phys.*, 115:236, 2001.

[12] D. J. Tannor. *Introduction to Quantum Mechanics: A Time Dependent Perspective*. University Science Books, 2007.

[13] R.W. Terhune. *Bull. Amer. Phys. Soc.*, 8:359, 1963.

[14] R.P.V. Duyne. *J. Electroanalytical Chem.*, 8:359, 1963.

[15] A. Otto. *Surface Science*, 75:L392, 1978.

[16] Kleinman et. al. *J. Am. Chem. Soc.*, 135:301, 2012.

[17] Wustholz et. al. *J. Am. Chem. Soc.*, 132:301, 2010.

[18] T.H. Wood M.V. Klein, D.A. Zwemer. *Surface Science*, 107:625, 1981.

[19] H. Seki. *J Vac Sci Tech*, 18:633, 1981.

[20] J. Creighton. *Surface Science*, 124:209, (1983).

[21] Moody et al. *App Spec*, 41:966, 1987.

[22] O. Martin J. Kottman. *Optics Express*, 8:655, 2001.

[23] Whitmore et. al. *J. Phys. Chem. C.*, 115:15900, 2011.

[24] C. Steuwe et al. *Nano Letters*, 11:5339, 2011.

[25] Apkarian et al. *J. Phys. Chem.*, 18:10415, 2012.

[26] V. Namboodiri et al. *Vib. Spec.*, 56:9, 2011.

[27] Apkarian et al. *ACS Nano*, 6:10343, 2012.

[28] Koo et al. *Opt. Lett.*, 30:1024, 2005.

[29] J.J. Baumberg S. Mahajan C. Steuwe, C.F. Kaminski. *Nano Lett*, 11:5339, 2011.

[30] Shen et al. *Phys. Rev. Lett.*, 43:943, 1979.

[31] M. Kerker H. Chew, D.S. Wang. *J. Opt. Soc. Am. B*, 1:1, 1984.

[32] N.G. Greeneltch R.P.V. Duyne D.L. Polla R.L. Aggarwal, L.W. Farrar. *App Spec*, 67: 2, 2013.

[33] Voronine et al. *Sci Rep*, 2:891, 2013.

[34] L. Novotny M. Danckwerts. *Phys. Rev. Lett.*, 98:026104, 2007.

[35] S. Lefrant I. Baltog, M. Baibarac. *Phys. Rev. B.*, 72:245402, 2005.

[36] Stolow et. al. *Science*, 314:278, 2006.

[37] H. W. Yang. *J. Chem. Phys.*, 104:4313, 1996.

[38] S. Mukamel. *Principles of Nonlinear Optical Spectroscopy.* Oxford University Press, 1995.

[39] Dieringer et. al. *J. Am. Chem. Soc.*, 129:16249, 2007.

[40] V. A. Apkarian I. U. Golschleger, M. N. van Staveren. *J. Chem. Phys.*, 139:034201, 2013.

[41] J. A. Cina T. S. Humble. *Ultrafast Proceedings*, 14:514, 2005.

[42] N. F. van Hulst R. Hildner, D. Brinks. *Nature Physics*, 7:172, 2011.

[43] Kneipp et. al. *Phys. Rev. Lett.*, 76:2444, 1996.

[44] D. A. Lidar V. A. Apkarian R. Zadoyan, D. Kohen. *Chem. Phys.*, 266:323, 2001.

[45] Glenn et. al. *Mol. Phys.*, 104:1249, 2006.

[46] Bihary et. al. *Chem. Phys. Lett*, 360:459, 2002.